"Rheo-NMR of transient and steady state shear banding under shear startup"

Rehab N. Al-kaby[1], Jayesha S. Jayaratne[2], Timothy I. Brox[3], Sarah L. Codd[1], Joseph D. Seymour[2] and Jennifer R. Brown[2]

[1]Department of Mechanical and Industrial Engineering, Montana State University, Bozeman MT 59717

[2] Department of Chemical and Biological Engineering, Montana State University, Bozeman MT 59717

[3] Victoria University of Wellington, SCPS, MacDiarmid Institute for Advanced Materials and Nanotechnology, Wellington, New Zealand

Receipt Date: (date manuscript received by the scientific editor)

Abstract

In this work shear band formation following shear startup as a function of flow protocol are investigated in the wormlike micelles (WLMs) system of 6 wt. % cetylpyridinium chloride (CPCl) and sodium salicylate (NaSal) in 0.5 M NaCl brine in a Couette Rheo-NMR shear cell. 1D velocity profiles across the 1 mm fluid gap are recorded every 1 s after shear startup using Rheo-NMR velocimetry and used to evaluate shear banding characteristics, including the shear rates in the low and high shear band, the interface position and the apparent wall slip. The velocity, and therefore the shear banding characteristics, exhibit large temporal fluctuations following an abrupt start-up to 12 s^{-1} due to apparent slip at the inner rotating wall and the presence of flow instabilities. Characteristic time scales were used to characterize the transition of the flow from transient to steady state and the Fourier transform of time autocorrelation functions was used to quantify fluctuation frequencies. Shear start-up experiments were performed for flow protocols with and without pre-shear. Pre-shear resulted in different magnitudes of the timescales and a shift in the frequencies of the fluctuation of all shear banding characteristics.

*corresponding author: jennifer.brown@montana.edu; 406-994-7719

Introduction

In an aqueous solution and under certain conditions, surfactant molecules can self-assemble into the semiflexible, elongated, and rod-shaped aggregates called wormlike micelles (WLMs) [19, 61]. At high enough concentrations, they form a viscoelastic entangled network similar to polymers but with an ability to dissociate and recombine dynamically [18]. In 1991, Rehage and Hoffmann [61] pointed out that some of those systems obey a robust Maxwellian viscoelastic model; *i.e.*, in contrast to polymer solutions that exhibit a wide range of relaxation times, they have a single relaxation time λ_R at small deformations [60]. This unique mechanical response time is predicted based on the reptation-reaction kinetics model in the fast-breaking regime, where the breaking and reformation events are faster than reptation [20]. Hence, the breakage and reptation relaxation mechanisms are characterized by the time scales of λ_{break} and λ_{rep}, respectively and the relaxation time is of the order $\sqrt{\lambda_{break}\lambda_{rep}}$ [63]. Due to the simple viscoelastic behavior of WLM systems and the fact that they are relatively easy to prepare and not generally susceptible to aging or degradation [24], they have become of significant interest for wide studies using different experimental techniques [17, 21, 67].

The nonlinear rheological behavior of WLMs is highly complex [24]. When subjected to shear stresses, semidilute and concentrated wormlike micelle solutions can exhibit an unusual mechanical response where the flow organizes into two macroscopic bands with distinct viscosities and local shear rates along the velocity gradient direction [40, 56]. This nonlinear transition is called shear banding and associated with the existence of a stress plateau in the steady state flow curve that occurs between two critical shear rates [5, 27]. Below the first critical shear rate $\dot{\gamma}_l$ and beyond the second critical shear rate $\dot{\gamma}_h$ the flow is homogeneous and the shear stress increases monotonically with the shear rate. Between the two critical shear rates, the flow becomes heterogeneous, forming shear bands, and stress stays nearly constant or varies slightly depending on the curvature of the flow geometry [35]. This plateau stress is independent of the flow history [6, 15]. When wall slip is negligible, the shear banded flow is usually assumed to follow a simple lever rule $\dot{\gamma}_a = \alpha\dot{\gamma}_h + (1-\alpha)\dot{\gamma}_l$, where $\dot{\gamma}_a$ is the applied shear rate, $\dot{\gamma}_h$ is the shear rate in the high shear band, $\dot{\gamma}_l$ is the shear rate in the low shear band and α is the proportion of the fluid gap occupied by the high shear rate, or the interface position. The high

and low shear rates, $\dot{\gamma}_h$ and $\dot{\gamma}_l$, correspond to the start and end of the stress plateau in the flow curve.

This nonlinear transition is widely observed in different complex fluids where applied shear changes the internal molecular microstructure and induces shear banding [9, 42, 49], including polymer solutions [64, 65], foams [37, 57], emulsions [58], colloidal glasses [22, 32], as well as in granular materials [48, 54]. Shear banding is thought to occur mainly due to the coupling of the microstructure and the flow field [38]. There is a rich literature that focuses on the shear-banding flow of wormlike micelles and their dynamics are well documented [4, 7] with experimental techniques like nuclear magnetic resonance NMR [11, 23, 47], particle image velocimetry PIV [35, 51], and ultrasonic velocimetry USV [1, 2]. Numerous early studies showed an interplay between wall slip and the shear banded flow in 1D velocity profiles [10, 31, 62]. Later experimental studies reported the existence of temporal fluctuations in the velocity [30, 44, 46, 50]. Most recently, 2D flow visualizations revealed that the shear banded flow is hydrodynamically unstable, resulting in development of secondary flows [25, 28, 52]. In the stress plateau, the instability manifests as vortices in the high shear band [29] that cause undulations in the interface position along the vorticial direction. Periodic or chaotic fluctuations observed previously in the velocity with 1D measurements could be attributed to the 3D nature of the flow field. Shear banded flow therefore involves not only temporal dynamics, but also a spatial heterogeneity.

As many of the applications using WLM solutions occur under time dependent conditions, such as startup or in complex geometries, work has been devoted to studying shear banding under time dependent flow protocols. For example, in *shear startup* is where an applied shear rate is imposed at a constant rate for all times $t > 0$ [36, 53], while in a *strain ramp*, the sample is sheared until a desired strain amplitude is reached [12, 59, 66]. A *step stress* protocol is performed by applying a constant stress for a certain amount of time [35, 45].

In this work, we use Rheo-NMR to obtain 1D velocity profiles across the fluid gap of a concentric cylinder shear cell as a function of time following *shear startup* at an applied shear rate within the stress plateau. We analyze the evolution of the shear banded flow from transient to steady state and the impact of pre-shear on the fluid response following the *shear startup*.

Materials and Methods

A. Sample preparation

The wormlike micelle system investigated in this work is a 6 wt. % cetylpyridinium chloride (CPCl) and sodium salicylate (NaSal) solution with a molar ratio [NaSal]/[CPCl] = 0.5 in 0.5 M NaCl-brine. Furthermore, 0.2 % $GdCl_3$ was added to reduce the ^1H NMR relaxation time to facilitate faster acquisition of NMR velocity profiles. The rheological measurements show that the addition of 0.2 % $GdCl_3$ had no noticeable influence on the mechanical behavior of the sample. All the materials were purchased from Sigma-Aldrich. The sample was prepared by mixing all components for 120 min at a temperature of 45 ˚C. The samples were then stored at 30 ˚C in a container preventing ambient light exposure conditions for at least 1 month before the experiments. This system has been extensively studied and is well-known to form elongated wormlike micelles [6].

B. Rheometry

The linear and nonlinear rheological measurements were performed using a TA instruments AR-G2 rheometer equipped with a steel cone-and-plate geometry with a 60 mm diameter and a 2˚ angle. Experiments were run at 25˚C and under a controlled strain. The linear viscoelastic measurement is shown in Figure 1, exhibiting a single mode Maxwellian behavior with characteristic relaxation time λ_R = 0.436 s and plateau modulus G_o = 100 Pa.

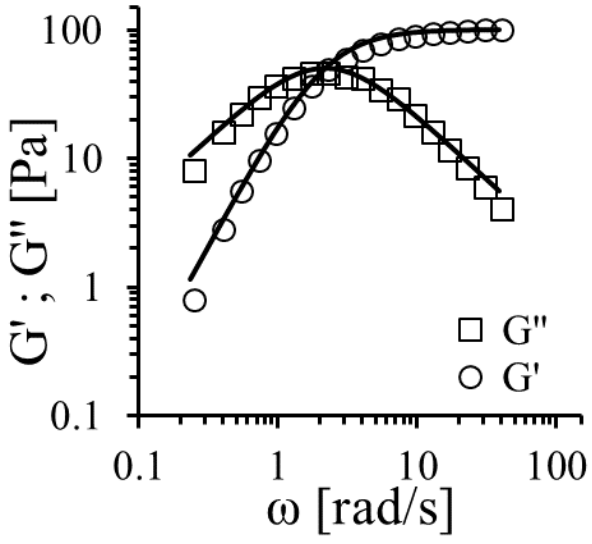

FIG 1. Storage and loss moduli as a function of frequency at a fixed 5% strain for 6 wt. % CPCl/NaSal in 0.5 M NaCl-brine. The data measured at T=25 °C using a cone-and-plate geometry. The solid lines are fits to the Maxwell model with λ_R = 0.436 s and G_o = 100 Pa.

This sample exhibits shear banding in the stress plateau region of the steady-state flow curve and a transient stress overshoot under *shear startup* within a few seconds [34, 35]. Figure 2 (a) and (b) show the nonlinear rheology of 6% CPCl/NaSal under the steady state and transient conditions respectively. The steady flow curve (Figure 2a) exhibits a stress plateau that extends from $\dot{\gamma}_l \approx 2.6$ s^{-1} to $\dot{\gamma}_h \approx 24$ s^{-1} as indicated by the dashed lines. The values of $\dot{\gamma}_l$ and $\dot{\gamma}_h$ were found by the same means as in Salmon *et al.* [62] and are in good agreement with those reported in the literature [25]. Figure 2b depicts the transient shear stress response after *shear startup* to $\dot{\gamma} = 12$ s^{-1}. The shear stress exhibits a significant overshoot (culminates up to 90 Pa) within a time less than 2 s, followed by a decrease until the steady-state value is obtained. However, a slow increase in stress just prior to steady state is observed, see inset Figure 2b. This dynamic feature is known as a "stress undershoot" and has been shown to appear in some cases after a critical shear rate [26]. To the best of our knowledge, the small undershoot has only been highlighted by Berret *et al.* [6] on different CPCl/NaSal/brine samples and by Lerouge and coworkers[43] on the wormlike micelle solution formed by the surfactant cetyltrimethylammonium bromide (CTAB).

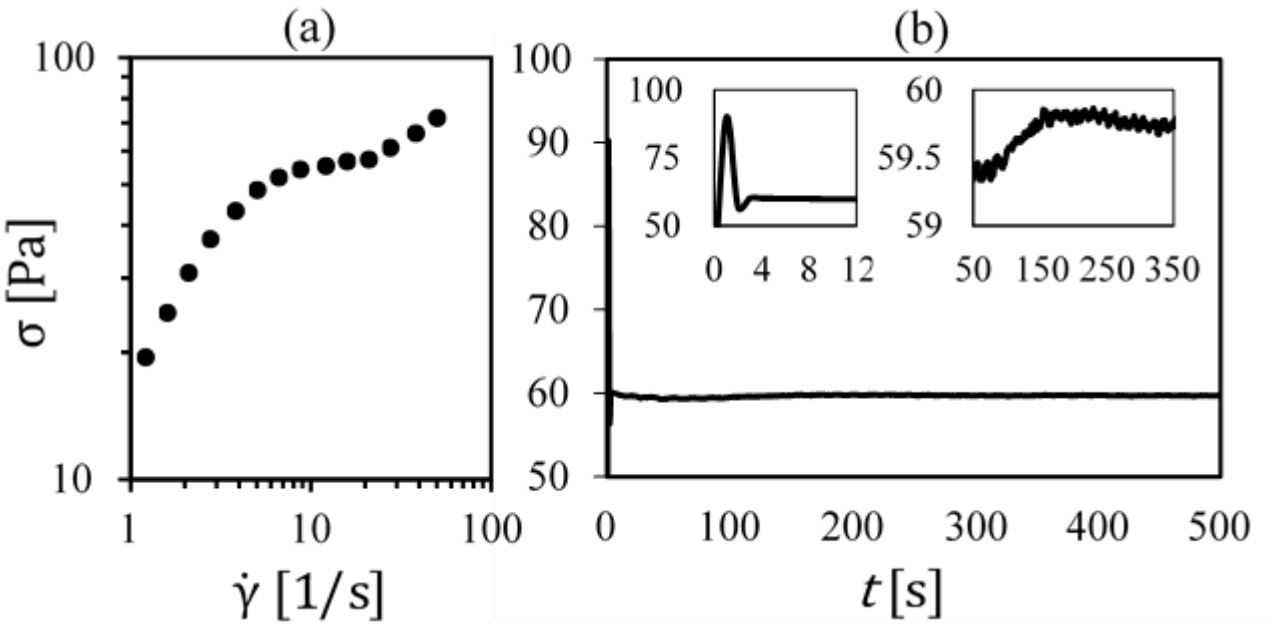

FIG 2. Bulk rheometry for 6% CPCl/NaSal wormlike micelle solution. (a) Stress vs applied shear rate exhibiting the stress plateau characteristic of shear banding that extends from $\dot{\gamma}_l \approx 2.6$ s^{-1} to $\dot{\gamma}_h \approx 24$ s^{-1} and (b) Stress as a function of time following *shear startup* to 12 s^{-1}. A large initial stress overshoot occurs in the first two seconds following *shear startup* and a small stress undershoot is observed at later times, as shown in the insets.

C. Rheo-NMR

Rheo-NMR experiments were performed in a Rheo-NMR Couette cell comprised of a glass stator and a polyether ether ketone (PEEK) rotor with a roughened cross hatched surface. The outer and inner radii of the shear cell were R_o = 9 and R_i = 8 mm, respectively, resulting in a fluid gap of 1 mm and a radius ratio ($\kappa = R_i / R_o$) of 0.89. All Rheo-NMR measurements are carried out at T = 22˚C, above the Krafft temperature of 21.5˚C.

A Bruker AVANCE 300 spectrometer equipped with a Micro-2.5 gradient system (maximum Gradient: 1.5 T/m 60A) and a 25 mm birdcage resonator coil, along with Bruker Topspin software, was used to acquire all Rheo-NMR data. The data analysis was performed using Prospa (Magritek, Wellington NZ) software. Pulsed gradient spin echo (PGSE) motion encoding was employed [16] with double slice selection and 1D image acquisition as depicted in

Figure 3 [14]. 1D velocity profiles were acquired across the fluid gap (velocity gradient direction; x-axis) with spatial resolution of 59 µm. The imaging region (Figure 3b) is a slab consisting of a 10 mm thick slice selected along the vorticity direction (z-axis) and a 1 mm thick slice along the velocity direction (y-axis). Velocity was measured in the direction of flow (y-axis) with displacement observation time Δ = 11 ms and magnatic field gradient pulse duration δ = 1 ms.

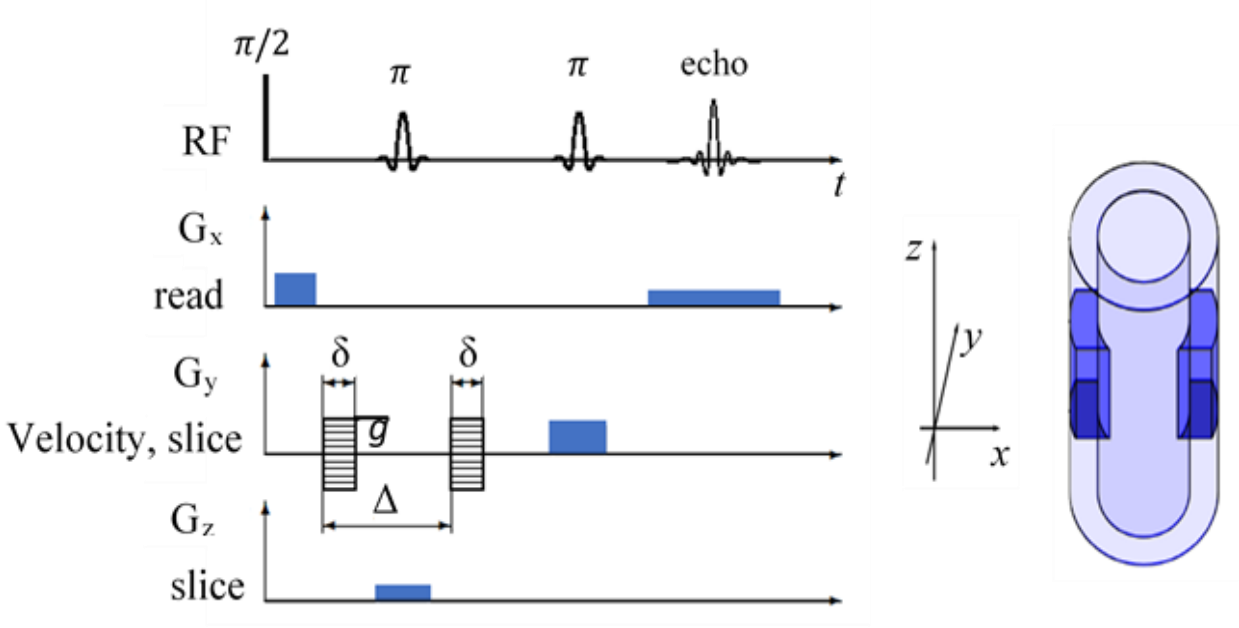

FIG 3. (a) Timing diagram for collecting a 1D velocity image across the fluid gap of the Couette cell using PGSE motion encoding with double slice selection. A 10 mm thick slice was selected along the vorticity direction (z-axis) and a 1 mm thick slice along the velocity direction (y-axis) in order to acquire data from the imaging region shown in the shaded section of the Couette schematic (b). The 1D image was acquired across the fluid gap in the velocity gradient direction (x-axis) with spatial resolution of 59 µm/pixel. Velocity was measured in the direction of flow (y-axis) with displacement observation time Δ = 11 ms and δ = 1 ms.

D. Experimental Protocols

In this work, we compare results from two different experimental protocols:

- Protocol 1 (no pre-shear): between each *shear startup* experiment, the sample was at rest for a wait time t_w = 300 min, in order to allow the system to return to an isotropic equilibrium state.
- Protocol 2 (with pre-shear): prior to each *shear startup* experiment, a pre-shear of 10 s^{-1} was applied for 1 min, followed by 2 min of rest. This protocol has been used previously in the literature in an attempt to ensure homogenization [45].

Results

In order to correlate the bulk mechanical stress response with the shear banding flow behavior of 6% CPCl/NaSal 1D velocity profiles are acquired across the fluid gap of a Rheo-NMR concentric cylinder Couette geometry under *shear startup* conditions. Figure 4a shows a representative *shear startup* experiment where 1D velocity profiles were acquired with a time resolution of 1 s following *shear startup* at 12 s^{-1}. There are fluctuations in the velocity with time as a consequence of apparent slip at the inner rotating wall and the presence of flow instabilities [25]. As this is a 1D measurement averaged over a 10 mm slice in the vorticial direction, the three dimensional flow due to axial velocity manifests as fluctuations in the measured velocity [25].

In the initial few seconds, corresponding to the large stress overshoot in the bulk mechanical response (Figure 2b), the velocity profile is linear (Figure 4b). The shear bands then begin to form, with the high shear band growing and the interface between the bands migrating further into the fluid gap until it reaches its steady state position. The steady state position can be roughly predicted with the lever rule as long as wall slip is not present.

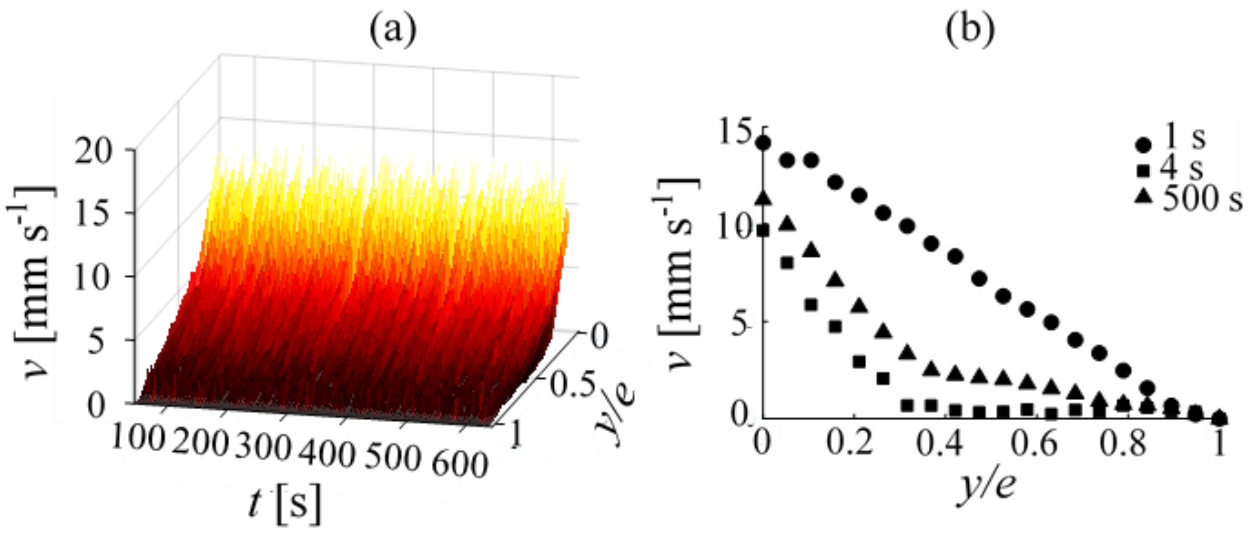

FIG 4. (a) 1D velocity profiles across the normalized fluid gap *y/e* as a function of time following *shear startup* at a shear rate of 12 s^{-1}, where *e* refers to the fluid gap width of 1 mm. The velocity fluctuates with time and exhibits apparent slip at the inner rotating wall. (b) 1D velocity profiles across the normalized fluid gap *y/e* at 1s, 4 s and 500 s after *shear startup*. The velocity at 1 s, prior to shear banding during the initial stress overshoot, exhibits a linear profile. By 4 s, shear bands have begun to form and the interface position is in the process of migrating from the inner rotating wall to its steady state position, shown for the profile at 500 s.

Here we identify timescales of the fluctuations in velocity and of the transient response. Even though we are limited by a 1D measurement, we attempt to extract information about the evolution of the flow from transient to steady state as well as about the instabilities that give rise to 3D flow by using a Reynolds decomposition approach [33], where we split the measured values into an average and the deviation from the average, *i.e*. the fluctuation. Since it is difficult to obtain velocity information with both high temporal and spatial resolution due to inherent limitations in the measurement methods, we choose to quantify and characterize the nature of both average quantities and the fluctuations in order to reveal insight into the flow behavior.

WLM solutions are known to exhibit memory. In other words, the fluid response depends on the shear history of a given sample [24, 55] and this will impact the transient response in particular [8]. To fully characterize the impact of shear history on the transient and steady state flow behavior, a protocol used by Lopez-Barron *et al.* [45] in a previous study utilizing pre-shear is compared to one for samples without any shear history.

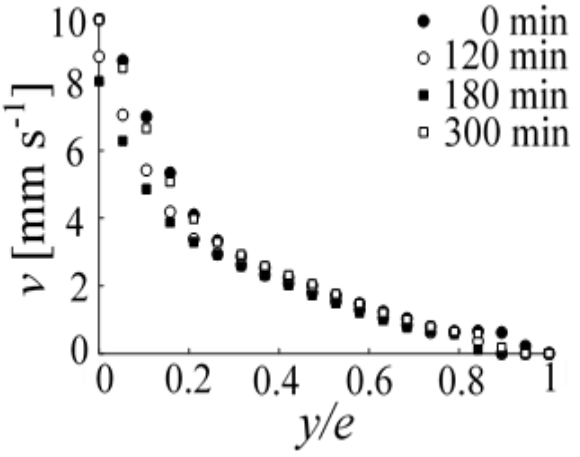

FIG 5. Velocity vs normalized fluid gap *y/e*. The 1D velocity profiles are time averaged over the last 2.12 min of the 10.6 min *shear startup* experiment to ensure the flow is at steady state and to average over fluctuations in the velocity. Profiles are shown for wait times t_w between experiments of 0 min (no shear history; filled circles), 120 min (open circles), 180 min (filled squares) and 300 min (open squares). After 300 min, the velocity profile overlays that for the sample without shear history, indicating a return to an equilibrium state.

To ensure that no shear history was present, *shear startup* experiments were performed with increasing wait time t_w between the experiments. The sample was assumed to be free of memory when no differences in the shear banded flow were observed as compared to the results from a fresh sample that had been at rest following sample loading into the Couette shear cell for > 12 hrs. Figure 5 shows 1D velocity profiles as a function of wait time across the fluid gap, time averaged over the last 2.12 min of the 10.6 min *shear startup* experiment to ensure the flow was

at steady state and to average over fluctuations in the velocity, as a function of wait time t_w. After 300 min wait time, the velocity profiles overlap exactly, indicating that the sample had returned fully to its equilibrium state at t_w=0.

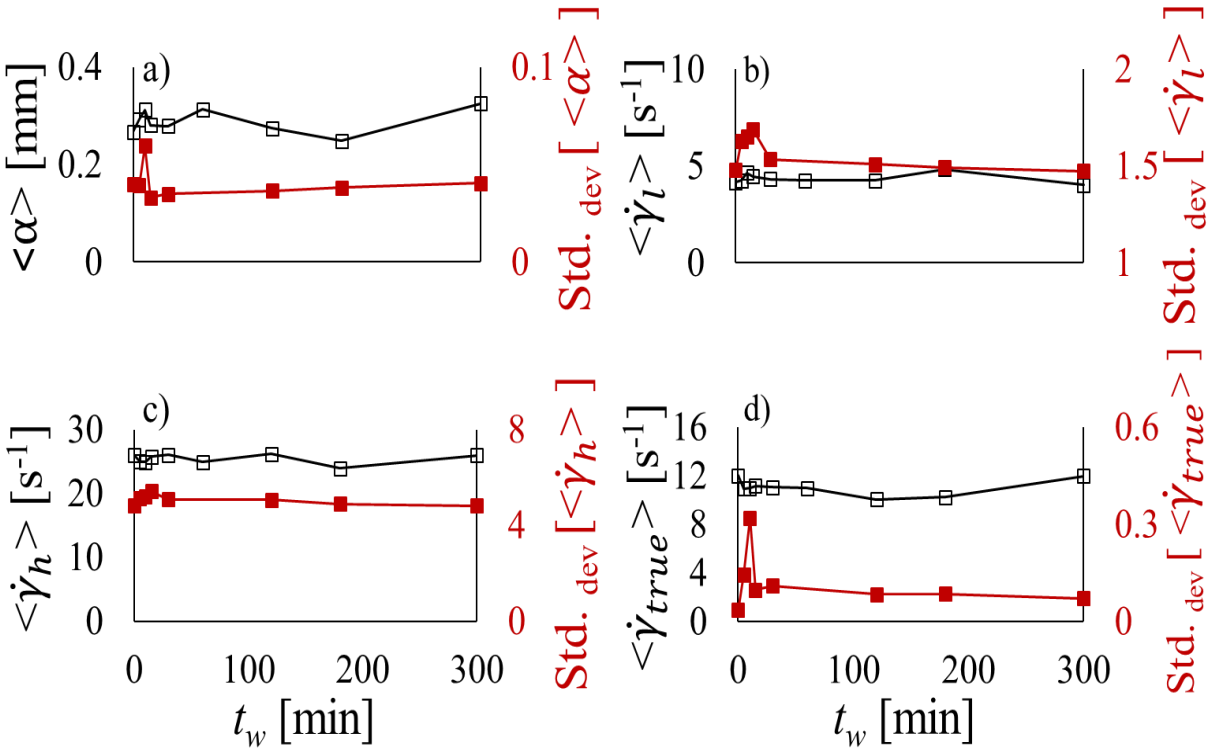

FIG 6. Shear banding characteristics (open symbols) and the standard deviation (closed symbols) as a function of wait time t_w. Lines are to guide the eye. (a) the interface position α (b) the shear rate in the low shear band $\dot{\gamma}_l$, (c) the shear rate in the high shear band $\dot{\gamma}_h$ and (d) the true shear rate $\dot{\gamma}_{true}$, which is a measure of apparent wall slip. The standard deviation becomes constant after 30 min.

To further evaluate how long a sample must be at rest to be rid of shear history, the velocity profiles were analyzed to quantify the characteristics of the shear banded flow. The shear rate in the high and low band, the interface position and the amount of apparent wall slip were monitored as a function of t_w. The regions of high and low shear in the 1D velocity profiles were fitted linearly with the slopes of the lines being the values of the shear rate $\dot{\gamma}_h$ and $\dot{\gamma}_l$ for the high

and low shear band respectively. The intersect of the lines was considered the interface position α and to evaluate the apparent wall slip, following Fardin *et al.* [26], a "true" shear rate $\dot{\gamma}_{true}$ was calculated as $\dot{\gamma}_{true}$ = |*v*(0)-*v*(*e*)|/*e* where *e* is the gap width. The shear banding characteristics obtained from the time averaged velocity profiles (as shown in Figure 5) are plotted in Figure 6 as a function of t_w. The values change the most significantly in the first 30 min. Also plotted in Figure 6 is the standard deviation from the average taken over the final 2.12 min of the experiment. After 30 min wait times, the standard deviation stays constant, another indication that shear history is having minimal impact on the characteristics of the flow.

While the individual velocity profiles we obtained didn't overlap exactly until t_w = 300 min, the primary characteristics of the flow (α, $\dot{\gamma}_h$, $\dot{\gamma}_l$, and $\dot{\gamma}_{true}$) stay the same after a t_w = 30 min, indicating the sample has returned to an equilibrium state (*i.e.* is no longer dependent on shear history) within 30 min. Experimental noise and sample to sample variation could account for small changes to the individual velocity profiles, so using the characteristics features of the flow seems a practical method to evaluate the impact of shear history. In the following results, a wait time of 300 min was used, but future studies could be made more time efficient by using a 30 min wait time.

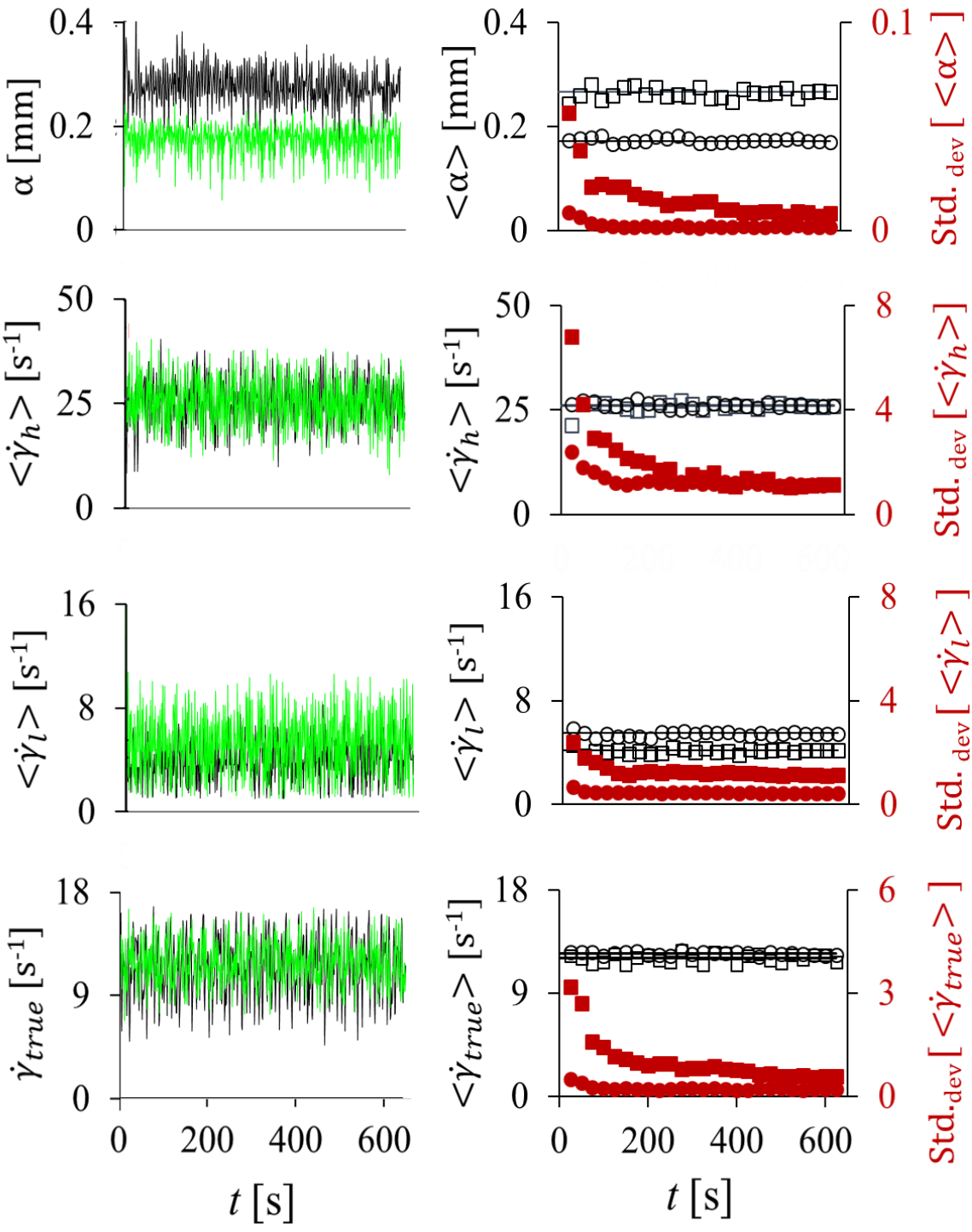
α [mm]
<α> [mm]
Std. dev [<α>]
<$\dot{\gamma}_h$> [s^{-1}]
Std. dev [<$\dot{\gamma}_h$>]
<$\dot{\gamma}_l$> [s^{-1}]
Std. dev [<$\dot{\gamma}_l$>]
$\dot{\gamma}_{true}$ [s^{-1}]
<$\dot{\gamma}_{true}$> [s^{-1}]
Std.dev [<$\dot{\gamma}_{true}$>]
t [s]

FIG 7. Left panels: top to bottom is the interface position α (a), the shear rate in the high shear band $\dot{\gamma}_h$ (c), the shear rate in the low shear band $\dot{\gamma}_l$ (e) and the true shear rate $\dot{\gamma}_{true}$ (g) obtained from 1D velocity profiles acquired every 1 s as a function of time following *shear startup* to 12 s^{-1}. The black line is protocol 1 (no shear history) and the green line is protocol 2 (with shear history). There are large fluctuations with time. Right panels: top to bottom is α (b), $\dot{\gamma}_h$ (d), $\dot{\gamma}_l$ (f), and $\dot{\gamma}_{true}$(h) averaged over 25 s, a timescale larger than that for the fluctuations. Protocol 1 are open black squares and protocol 2 are open black circles. Solid lines represent the average values for the entire experiment (Protocol 1: $\dot{\gamma}_h$= 26 s^{-1}, $\dot{\gamma}_l$ =4.2 s^{-1}, α =0.27 and $\dot{\gamma}_{true} = 12$ s^{-1}; Protocol 2: $\dot{\gamma}_h$= 26 s^{-1}, $\dot{\gamma}_l$ =5.5 s^{-1}, α =0.17 and $\dot{\gamma}_{true} =$ 12.5 s^{-1}). Closed red symbols are the standard deviations within each 25 s period. For protocol 1, the standard deviation decreases rapidly in early times (t < 75 s), then at a slower rate (until t ~200-400 s) and finally is minimized (t > 400 s). For protocol 2, the standard deviation rapidly decreases to reach its minimal value by t = 100 s.

The left panels of Figure 7 show the primary characteristics of the flow (α, $\dot{\gamma}_h$, $\dot{\gamma}_l$, and $\dot{\gamma}_{true}$) obtained from 1D velocity profiles acquired every 1 s following abrupt *shear startup* to 12 s^{-1} (Figure 4) for *shear startup* protocols without pre-shear (protocol 1) and with pre-shear (protocol 2). The velocity, and therefore corresponding shear banding characteristics, show large fluctuations with time due to apparent slip and hydrodynamic instabilities. Taking a Reynolds decomposition approach [33], where variables are decomposed into a time-averaged quantity and a fluctuation about the time average, the velocity profiles were averaged over 25 s and the shear banding characteristics for these profiles are plotted in the right panels of Figure 7. The closed symbols are the coarse-grained time averaged values of the shear banding characteristics, while the solid lines are the average over the entire experiment. This approach was taken in order to extract any timescales in the system for characterizing the evolution from transient to steady state that are obscured by the fluctuations. As with any coarse graining approach, the averaging time must be carefully selected to be longer than the fluctuation timescale τ_f, but shorter than any other timescale that would yield information. Also shown (red closed symbols) is the standard deviation of the 25 s time averaged values from the overall mean. The standard deviation more clearly reveals the changes in the shear banding characteristics with time.

As noted previously, shear bands begin to form after the first 2 seconds (Figure 4b), corresponding to the initial large stress overshoot (Figure 2b). The interface position then

migrates to its steady state position within the fluid gap. We define the timescale for this interface migration as the transient timescale τ_{trans}. Previous work has similarly shown linear velocity profiles during the stress overshoot [35, 44] and identified a long lived "metastable" state several hundred seconds long, where the interface position migrates to its steady state position and flow instabilities develop prior to settling into a steady state [28]. We define the timescale to reach this steady state as τ_{ss}. During the metastable regime, several features of the stress have been observed [3, 41], including a stress undershoot [39] as observed for the system for a *shear startup* at 12 s^{-1} (Figure 2b).

The metastable regime could be broken down into several parts, each with different features in the stress and the flow behavior. Shear bands form and the interface position migrates from the inner wall farther into the fluid gap within the first 50-75 s (Figure 7). This migration is seen in both Figure 7a and 7b as the interface position increases with timescale τ_{trans}~=50-75 s. This is also more clearly demonstrated in the standard deviation, which decreases rapidly during this time. Beyond ~75 s, the interface position appears to reach the steady state mean value (the solid line), but also fluctuates or oscillates about that mean. This is reflected in a more gradual decrease in the standard deviation until ~300-400 s, where it finally plateaus to a minimum value. The slowly decreasing deviation from the mean would correspond to the metastable state where the stress undershoot occurs, which has been deemed a mechanical signature of the onset and development of flow instabilities [43]. The minimization of the standard deviation indicates that the overall flow behavior, despite the presence of 3D flow from instabilities and the resulting velocity fluctuations in a 1D measurement, is no longer changing with time and we have reached a steady state. Therefore, the steady state timescale τ_{ss}~= 300-400 s. This behavior is reflected in $\dot{\gamma}_h$, $\dot{\gamma}_l$, and $\dot{\gamma}_{true}$ as well as α. It can be seen most clearly by looking at the standard deviation of the time averaged values (right panels, Figure 7).

It is expected that the transient and steady state timescales would depend on multiple factors, such as the geometry of the shear cell, the applied shear rate, and shear history to name a few. They should also depend on the properties of the sample, such as the relaxation time τ_r, the time it takes for a single chain to relax back to its equilibrium state after being out of equilibrium, which is a function of surfactant and counter-ion concentration as well as temperature.

Comparing protocol 1 (no shear history) with protocol 2 (with pre-shear), we see that the standard deviation of α, $\dot{\gamma}_h$, $\dot{\gamma}_l$, and $\dot{\gamma}_{true}$ is minimized within the first 50-75 s for protocol 2. It appears as though the transient timescale is now equal to the steady state timescale. With pre-shear, the microstructure of the sample is presumably disturbed, which may have allowed the hydrodynamic instabilities to develop more rapidly, bypassing a "metastable" state as observed in previous studies [25, 39, 43].

In addition, several of the shear banding characteristics are changed. The average interface position goes from 0.27 in protocol 1 to 0.17 (nearer to the inner rotating wall of the Couette) in protocol 2 where pre-shear occurred. The average value of the low shear rate $\dot{\gamma}_l$ increased from 4.2 s^{-1} in protocol 1 to 5.5 s^{-1} in protocol 2. The high shear rate $\dot{\gamma}_h$ and amount of apparent wall slip, as indicated by the value of $\dot{\gamma}_{true}$, however, were roughly the same (26 s^{-1} and 12 s^{-1} respectively). Significant wall slip is not observed in either protocol. It appears there is a compensation mechanism, in which when the interface position is located farther in the fluid gap (protocol 1 without pre-shear), the value for the low shear rate is smaller.

To extract information about the 3D flow instabilities during the various regimes observed in the stress response and shear banded flow behavior, we further analyze the fluctuations. The fluctuations are not random but reflect the coherent 3D nature of the flow. Previously, the Fourier transform of Rheo-NMR velocimetry data [13] and velocity autocorrelation functions [46] were used to analyze velocity fluctuations in wormlike micelle systems. Here, we Fourier Transform time autocorrelation functions of the four characteristics of shear banding to obtain power spectra, which is a standard analysis and has the advantage over direct Fourier transform of reducing noise in the resulting spectra. The time domain data was divided into 64 s time intervals following *shear startup* and was used to calculate time autocorrelation functions, which were then Fourier transformed to obtain the spectra in Figures 8 and 9 (α and $\dot{\gamma}_h$ in Figure 8 and $\dot{\gamma}_l$ and $\dot{\gamma}_{true}$ in Figure 9). These spectra quantify the fluctuations corresponding to the various regimes inferred from both the stress response and flow behavior observed in the velocity profiles: in the initial interface migration phase (the time following the stress overshoot at 2 to ~50-75 s), during the metastable regime (from 2 to ~300-400 s) and when the flow has reached steady state (time after start up >400 s). We clearly observe different frequencies depending upon the particular characteristic of shear banding and between the two flow protocols.

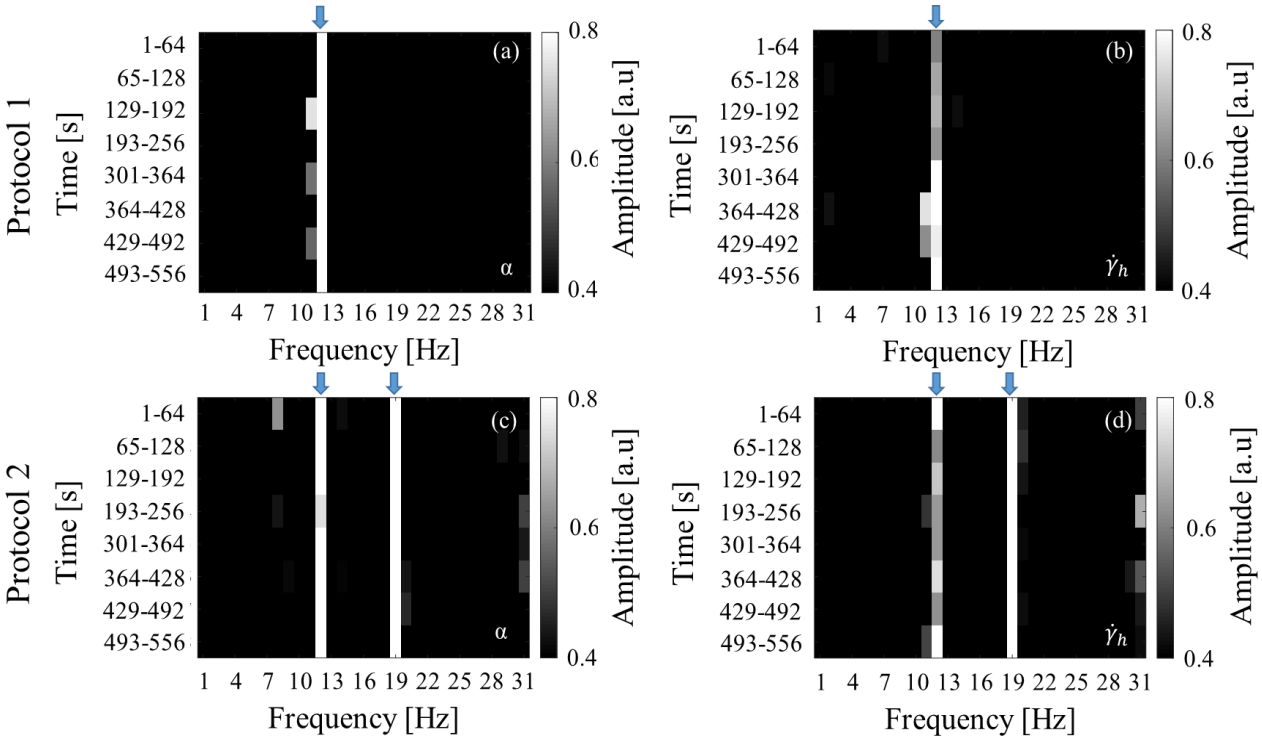

FIG 8. Frequency images from the Fourier transform of the time correlation functions. The colorbars correspond to amplitude (intensity normalized by the maximum intensity) in arbitrary units (a.u.). (a, c) interface position for protocol 1 (a) and protocol 2 (c). The dominant frequencies in the spectra are shown with blue arrows. In protocol 1, there is one frequency at 12 Hz that occurs for all times following *shear startup* to 12 s^{-1}. For protocol 2, there are two frequencies at 12 and 19 Hz. (b, d) high shear rate for protocol 1 (b) and protocol 2 (d). The same frequencies for protocol 1 (12 Hz) and protocol 2 (12 and 19 Hz) are observed in the spectra for the high shear rate.

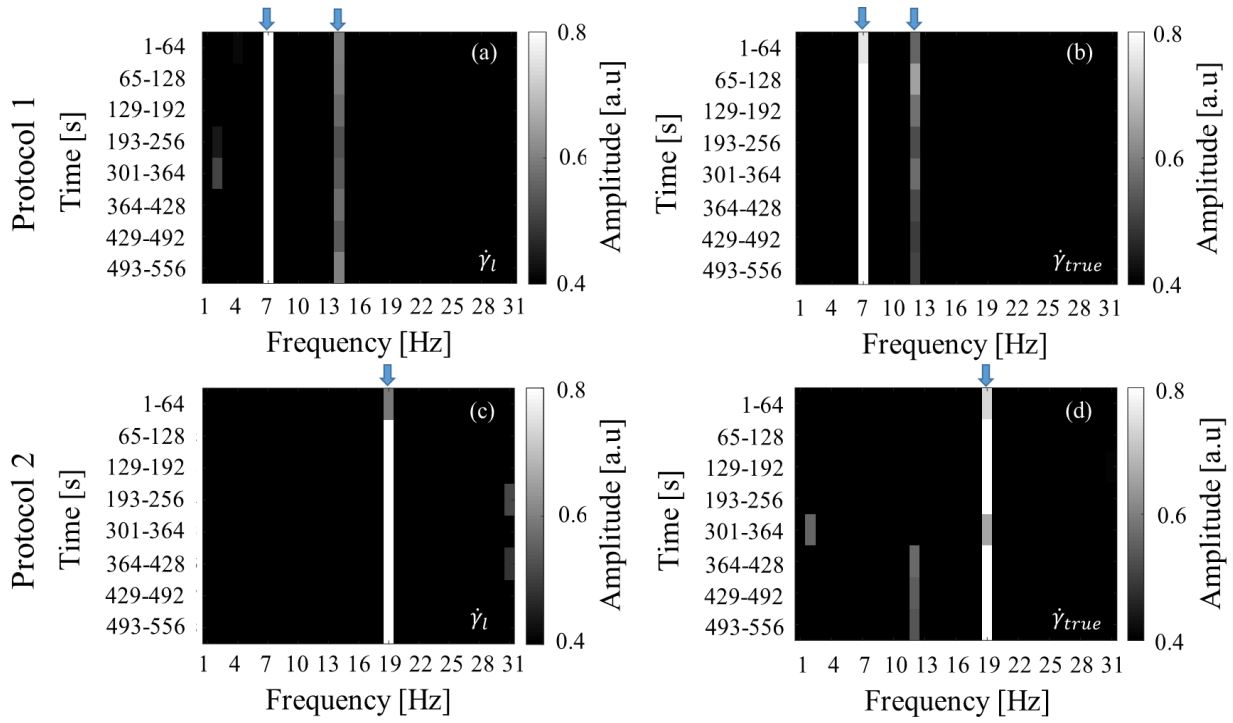

FIG 9. Frequency images from the Fourier transform of the time autocorrelation functions. The colorbars correspond to amplitude (intensity normalized by the maximum intensity) in arbitrary units (a.u.). (a, c) low shear rate for protocol 1 (a) and protocol 2 (c). The dominant frequencies in the spectra are shown with blue arrows. In protocol 1, there are frequencies at 7 and 14 Hz that occur for all times following *shear startup* to 12 s^{-1}. For protocol 2, there is a single dominant frequency at 19 Hz. (b, d) the true shear rate for protocol 1 (b) and protocol 2 (d). Similar frequencies are observed for protocol 1 (7 and 12 Hz) and protocol 2 (19 Hz).

For protocol 1, there is nearly a universal frequency of 12 Hz present at all times following *shear startup* and in all characteristics of shear banding (in the low shear rate there is a small shift to 14 Hz). However, a second high intensity frequency of 7 Hz is present in the low and true shear rates. There appears to be correlation between the interface and high shear rate fluctuations and the low shear rate and true shear rate fluctuations. The appearance of a strong lower second frequency in low shear rate and true shear rate indicates a coupling between slip and low shear rate. For protocol 2, there is a universal frequency of 19 Hz present at all times

and in all of the characteristics of shear banding. A second frequency of 12 Hz of roughly similar intensity occurs in the interface position and high shear rate, indicating a coupling between these two values.

In general, we see correlations between fluctuations of the high shear rate and interface position, as well as between fluctuations of low shear rate and apparent wall slip (seen through the true shear rate). Comparing the two protocols, we see a shift in the frequency universal to all shear banding characteristics. With Protocol 2 that involved a short wait time and pre-shear, the universal frequency is higher (19 Hz) than with Protocol 1 where a long wait time and no pre-shear was emplyed (12 Hz). A second, high intensity frequency presents itself in the low shear rate and true shear rate for protocol 1 (7 Hz). In protocol 2, a second equal intensity frequency appears in the high shear rate and interface position at a higher value (12 Hz). Interestingly, the frequency values do not shift depending on the regime (time after *shear startup*). Data for a range of applied shear rates is needed to correlate these frequencies to the specific nature of the hydrodynamic instabilities and the resulting secondary flows and research is currently ongoing in this direction.

Conclusions

Shear banding following *shear startup* was studied in a solution of wormlike micelles (WLMs) by measuring 1D velocity profiles across the 1 mm fluid gap of a Rheo-NMR concentric cylinder Couette cell using Rheo-NMR velocimetry. Fits to the velocity profiles were used to evaluate the shear banding characteristics, including the shear rates in the low and high shear band, the interface position and the true shear rate. Measurements were made for two flow protocols, one with and one without pre-shear. Due to the presence of flow instabilities, large temporal fluctuations were observed in the flow characteristics obtained from a 1D measurement. Extending the spatial dimension to 2D would sacrifice temporal resolution, therefore, we instead separated the averaged quantities from the fluctuations about the average and analyzed them separately. The timescales for the flow to transition from a transient response to steady state were identified and quantified from analysis of the average values. The fluctuations were quantified through Fourier Transform of the time correlation functions of the data to obtain spectra of fluctuation frequencies. Pre-shear resulted in different magnitudes of

the timescales and a shift in the frequencies of the fluctuation of all shear banding characteristics. Further experiments are needed to elucidate the connection between these frequencies and the nature of the hydrodynamic instabilities.

Acknowledgements

JRB acknowledges the NSF (1543875) for funding. RA acknowledges the Higher Committee for Education Development in Iraq (HREC) for fellowship funding. JRB, SLC and JDS acknowledge the M. J. Murdoch charitable trust for equipment funding.

References

[1] Becu, L., Anache, D., Manneville, S., and Colin, A., ‘‘Evidence for three-dimensional unstable flows in shear-banding wormlike micelles,’’ Physical Review E 76 (2007).
[2] Bécu, L., Manneville, S., and Colin, A., ‘‘Spatiotemporal dynamics of wormlike micelles under shear,’’ Physical review letters 93, 018301 (2004).
[3] Berret, J.-F., ‘‘Transient rheology of wormlike micelles,’’ Langmuir 13, 2227-2234 (1997).
[4] Berret, J.-F., “Rheology of wormlike micelles: equilibrium properties and shear banding transitions.” *Molecular gels* (Springer, 2006).
[5] Berret, J.-F., Roux, D., and Lindner, P., ‘‘Structure and rheology of concentrated wormlike micelles [4] at the shear-induced isotropic-to-nematic transition,’’ The European Physical Journal B-Condensed Matter and Complex Systems 5, 67-77 (1998).
[6] Berret, J.-F., Roux, D. C., and Porte, G., ‘‘Isotropic-to-nematic transition in wormlike micelles under shear,’’ Journal de Physique II 4, 1261-1279 (1994).
[7] Berret, J.-F. c., Porte, G., and Decruppe, J.-P., ‘‘Inhomogeneous shear flows of wormlike micelles: mA master dynamic phase diagram,’’ Physical Review E 55, 1668 (1997).
[8] Berret, J. F., Gamez-Corrales, R., Lerouge, S., and Decruppe, J. P., ‘‘Shear-thickening transition in surfactant solutions: New experimental features from rheology and flow birefringence,’’ European Physical Journal E 2, 343-350 (2000).
[9] Boukany, P. E., and Wang, S. Q., ‘‘Exploring the transition from wall slip to bulk shearing banding in well-entangled DNA solutions,’’ Soft Matter 5, 780-789 (2009).
[10] Britton, M., and Callaghan, P., ‘‘Shear banding instability in wormlike micellar solutions,’’ The European Physical Journal B-Condensed Matter and Complex Systems 7, 237-249 (1999).
[11] Britton, M. M., and Callaghan, P. T., ‘‘Two-phase shear band structures at uniform stress,’’ Physical Review Letters 78, 4930-4933 (1997).
[12] Brown, E., Burghardt, W., and Venerus, D., ‘‘Tests of the Lodge− Meissner Relation in Anomalous Nonlinear Step Strain of an Entangled Wormlike Micelle Solution,’’ Langmuir 13, 3902-3904 (1997).

[13] Brown, J. R., and Callaghan, P. T., ‘‘Changing micellar order, lever rule behavior and spatio-temporal dynamics in shear-banding at the onset of the stress plateau,’’ Soft Matter 7, 10472-10482 (2011).
[14] Brox, T. I., Douglass, B., Galvosas, P., and Brown, J. R., ‘‘Observations of the influence of Taylor-Couette geometry on the onset of shear-banding in surfactant wormlike micelles,’’ Journal of Rheology 60, 973-982 (2016).
[15] Callaghan, P., Cates, M., Rofe, C., and Smeulders, J., ‘‘A Study of the “Spurt Effect" in Wormlike Micelles Using Nuclear Magnetic Resonance Microscopy,’’ Journal de Physique II 6, 375-393 (1996).
[16] Callaghan, P. T., *Translational Dynamics and Magnetic Resonance: Principles of Pulsed Gradient Spin Echo NMR* (Oxford University Press, New York, 2011).
[17] Candau, S., and Oda, R., ‘‘Linear viscoelasticity of salt-free wormlike micellar solutions,’’ Colloids and Surfaces A: Physicochemical and Engineering Aspects 183, 5-14 (2001).
[18] Cates, M., ‘‘Nonlinear viscoelasticity of wormlike micelles (and other reversibly breakable polymers),’’ Journal of Physical Chemistry 94, 371-375 (1990).
[19] Cates, M., and Candau, S., ‘‘Statics and dynamics of worm-like surfactant micelles,’’ Journal of Physics: Condensed Matter 2, 6869 (1990).
[20] Cates, M. E., ‘‘Reptation of living polymers: dynamics of entangled polymers in the presence of reversible chain-scission reactions,’’ Macromolecules 20, 2289-2296 (1987).
[21] Cates, M. E., and Evans, M. R., *Soft and fragile matter: nonequilibrium dynamics, metastability and flow (PBK)* (CRC Press, 2000).
[22] Coussot, P., Raynaud, J., Bertrand, F., Moucheront, P., Guilbaud, J., Huynh, H., Jarny, S., and Lesueur, D., ‘‘Coexistence of liquid and solid phases in flowing soft-glassy materials,’’ Physical review letters 88, 218301 (2002).
[23] Douglass, B. S., Colby, R. H., Madsen, L. A., and Callaghan, P. T., ‘‘Rheo-NMR of wormlike micelles formed from nonionic pluronic surfactants,’’ Macromolecules 41, 804-814 (2008).
[24] Dusek, K., “Polymer Characterization: Rheology, Laser Interferometry, Electrooptics,” in Editor (ed)^(eds). *Book Polymer Characterization: Rheology, Laser Interferometry, Electrooptics* (Berlin, Heidelberg : Springer Berlin Heidelberg : Imprint: Springer, Berlin ; Heidelberg ; New York, 2010).
[25] Fardin, M.-A., Casanellas, L., Saint-Michel, B., Manneville, S., and Lerouge, S., ‘‘Shear-banding in wormlike micelles: Beware of elastic instabilities,’’ Journal of Rheology 60, 917-926 (2016).
[26] Fardin, M.-A., and Lerouge, S., ‘‘Instabilities in wormlike micelle systems,’’ The European Physical Journal E 35, 1-29 (2012).
[27] Fardin, M.-A., and Lerouge, S., ‘‘Flows of living polymer fluids,’’ Soft Matter 10, 8789-8799 (2014).
[28] Fardin, M. A., Divoux, T., Guedeau-Boudeville, M. A., Buchet-Maulien, I., Browaeys, J., McKinley, G. H., Manneville, S., and Lerouge, S., ‘‘Shear-banding in surfactant wormlike micelles: elastic instabilities and wall slip,’’ Soft Matter 8, 2535-2553 (2012).
[29] Fardin, M. A., Lasne, B., Cardoso, O., Gregoire, G., Argentina, M., Decruppe, J. P., and Lerouge, S., ‘‘Taylor-like Vortices in Shear-Banding Flow of Giant Micelles,’’ Physical Review Letters 103, 4 (2009).
[30] Feindel, K. W., and Callaghan, P. T., ‘‘Anomalous shear banding: multidimensional dynamics under fluctuating slip conditions,’’ Rheologica Acta 49, 1003-1013 (2010).

[31] Fischer, E., and Callaghan, P. T., ‘‘Is a birefringence band a shear band?,’’ Europhysics Letters 50, 803-809 (2000).
[32] Gibaud, T., Barentin, C., and Manneville, S., ‘‘Influence of boundary conditions on yielding in a soft glassy material,’’ Physical Review Letters 101, 258302 (2008).
[33] Glasgow, L. A., *Transport phenomena: an introduction to advanced topics* (John Wiley & Sons, 2010).
[34] Helgeson, M. E., Vasquez, P. A., Kaler, E. W., and Wagner, N. J., ‘‘Rheology and spatially resolved structure of cetyltrimethylammonium bromide wormlike micelles through the shear banding transition,’’ Journal of Rheology 53, 727-756 (2009).
[35] Hu, Y. T., and Lips, A., ‘‘Kinetics and mechanism of shear banding in an entangled micellar solution,’’ Journal of Rheology 49, 1001-1027 (2005).
[36] Hu, Y. T., Palla, C., and Lips, A., ‘‘Comparison between shear banding and shear thinning in entangled micellar solutions,’’ Journal of Rheology 52, 379-400 (2008).
[37] Krishan, K., and Dennin, M., ‘‘Viscous shear banding in foam,’’ Physical Review E 78, 051504 (2008).
[38] Larson, R. G., *The Structure and Rheology of Complex Fluids* (Oxford University Press, New York, 1999).
[39] Lerouge, S., Argentina, M., and Decruppe, J. P., ‘‘Interface instability in shear-banding flow,’’ Physical Review Letters 96, 4 (2006).
[40] Lerouge, S., and Berret, J.-F., “Shear-induced transitions and instabilities in surfactant wormlike micelles.” *Polymer Characterization* (Springer, 2009).
[41] Lerouge, S., Decruppe, J. P., and Berret, J. F., ‘‘Correlations between rheological and optical properties of a micellar solution under shear banding flow,’’ Langmuir 16, 6464-6474 (2000).
[42] Lerouge, S., Decruppe, J. P., and Olmsted, P., ‘‘Birefringence banding in a micellar solution or the complexity of heterogeneous flows,’’ Langmuir 20, 11355-11365 (2004).
[43] Lerouge, S., Fardin, M. A., Argentina, M., Gregoire, G., and Cardoso, O., ‘‘Interface dynamics in shear-banding flow of giant micelles,’’ Soft Matter 4, 1808-1819 (2008).
[44] Lettinga, M. P., and Manneville, S., ‘‘Competition between Shear Banding and Wall Slip in Wormlike Micelles,’’ Physical Review Letters 103 (2009).
[45] Lopez-Barron, C. R., Gurnon, A. K., Eberle, A. P. R., Porcar, L., and Wagner, N. J., ‘‘Microstructural evolution of a model, shear-banding micellar solution during shear startup and cessation,’’ Physical Review E 89 (2014).
[46] Lopez-Gonzalez, M. R., Holmes, W. M., and Callaghan, P. T., ‘‘Rheo-NMR phenomena of wormlike micelles,’’ Soft Matter 2, 855-869 (2006).
[47] Lopez-Gonzalez, M. R., Holmes, W. M., Callaghan, P. T., and Photinos, P. J., ‘‘Shear Banding Fluctuations and Nematic Order in Wormlike Micelles,’’ Physical Review Letters 93, 268-302 (2004).
[48] Losert, W., Bocquet, L., Lubensky, T. C., and Gollub, J. P., ‘‘Particle dynamics in sheared granular matter,’’ Physical Review Letters 85, 1428-1431 (2000).
[49] Manneville, S., ‘‘Recent experimental probes of shear banding,’’ Rheologica Acta 47, 301-318 (2008).
[50] Manneville, S., Bécu, L., and Colin, A., ‘‘High-frequency ultrasonic speckle velocimetry in sheared complex fluids,’’ The European Physical Journal-Applied Physics 28, 361-373 (2004).
[51] Miller, E., and Rothstein, J. P., ‘‘Transient evolution of shear-banding wormlike micellar solutions,’’ Journal of Non-Newtonian Fluid Mechanics 143, 22-37 (2007).

[52] Mohammadigoushki, H., and Muller, S. J., ‘‘Inertio-elastic instability in Taylor-Couette flow of a model wormlike micellar system,’’ Journal of Rheology 61, 683-696 (2017).
[53] Moorcroft, R. L., and Fielding, S. M., ‘‘Shear banding in time-dependent flows of polymers and wormlike micelles,’’ Journal of Rheology 58, 103-147 (2014).
[54] Mueth, D. M., Debregeas, G. F., Karczmar, G. S., Eng, P. J., Nagel, S. R., and Jaeger, H. M., ‘‘Signatures of granular microstructure in dense shear flows,’’ Nature 406, 385 (2000).
[55] Oelschlaeger, C., Waton, G., Candau, S., and Cates, M., ‘‘Structural, kinetics, and rheological properties of low ionic strength dilute solutions of a dimeric (gemini) surfactant,’’ Langmuir 18, 7265-7271 (2002).
[56] Olmsted, P. D., ‘‘Perspectives on shear banding in complex fluids,’’ Rheologica Acta 47, 283-300 (2008).
[57] Ovarlez, G., Krishan, K., and Cohen-Addad, S., ‘‘Investigation of shear banding in three-dimensional foams,’’ EPL (Europhysics Letters) 91, 68005 (2010).
[58] Paredes, J., Shahidzadeh-Bonn, N., and Bonn, D., ‘‘Shear banding in thixotropic and normal emulsions,’’ Journal of Physics: Condensed Matter 23, 284116 (2011).
[59] Pipe, C., Kim, N., Vasquez, P., Cook, L., and McKinley, G., ‘‘Wormlike micellar solutions: II. Comparison between experimental data and scission model predictions,’’ Journal of Rheology 54, 881-913 (2010).
[60] Rehage, H., and Hoffmann, H., ‘‘Rheological properties of viscoelastic surfactant systems,’’ The Journal of Physical Chemistry 92, 4712-4719 (1988).
[61] Rehage, H., and Hoffmann, H., ‘‘Viscoelastic surfactant solutions: model systems for rheological research,’’ Molecular Physics 74, 933-973 (1991).
[62] Salmon, J. B., Colin, A., Manneville, S., and Molino, F., ‘‘Velocity profiles in shear-banding wormlike micelles,’’ Physical Review Letters 90 (2003).
[63] Spenley, Cates, and McLeish, ‘‘Nonlinear rheology of wormlike micelles,’’ Physical review letters 71, 939 (1993).
[64] Sprakel, J., Spruijt, E., Stuart, M. C., Besseling, N., Lettinga, M., and van der Gucht, J., ‘‘Shear banding and rheochaos in associative polymer networks,’’ Soft Matter 4, 1696-1705 (2008).
[65] Tapadia, P., and Wang, S.-Q., ‘‘Yieldlike constitutive transition in shear flow of entangled polymeric fluids,’’ Physical review letters 91, 198301 (2003).
[66] Vasquez, P. A., McKinley, G. H., and Cook, L. P., ‘‘A network scission model for wormlike micellar solutions: I. Model formulation and viscometric flow predictions,’’ Journal of non-newtonian fluid mechanics 144, 122-139 (2007).
[67] Yang, J., ‘‘Viscoelastic wormlike micelles and their applications,’’ Current opinion in colloid & interface science 7, 276-281 (2002).